# Weakened AMOC upper limb compensated by strengthened South Atlantic subtropical gyre circulation in CESM1-LE simulations

Fernanda Marcello*[1,2], Marcos Tonelli[1,3], Bruno Ferrero[1] and Ilana Wainer[1]

*fernanda.marcello@usp.br

[1]Oceanographic Institute of the University of São Paulo (IO-USP) — São Paulo, Brazil

[2]Laboratorie d'océanographie et du climat (LOCEAN) - Sorbonne Université — Paris, France

[3]Admiral Paulo Moreira Institute for Marine Studies (IEAPM) — Brazilian Navy - Arraial do Cabo, RJ, Brazil

Fernanda Marcello – post-doctoral researcher

MSc (2017), PhD (2021) Physical Oceanography

- **IO-USP** – Oceanographic Institute, University of São Paulo, Brazil
- **LOCEAN** – Sorbonne University, Paris, France. *(current institution)

Published online as:

communications earth & environment

ARTICLE

https://doi.org/10.1038/s43247-023-00750-4 OPEN

## Projected Atlantic overturning slow-down is to be compensated by a strengthened South Atlantic subtropical gyre

Fernanda Marcello [1✉], Marcos Tonelli [1,2], Bruno Ferrero [1] & Ilana Wainer [1]

- Link to blog post *Behind the Paper*

(also pointing to the article page):

https://earthenvironmentcommunity.nature.com/posts/ocean-circulation-changes-in-a-warming-climate-the-south-atlantic-coupled-response-to-wind-and-thermohaline-forcings

# Weakened AMOC upper limb compensated by strengthened South Atlantic subtropical gyre in CESM1-LE simulations

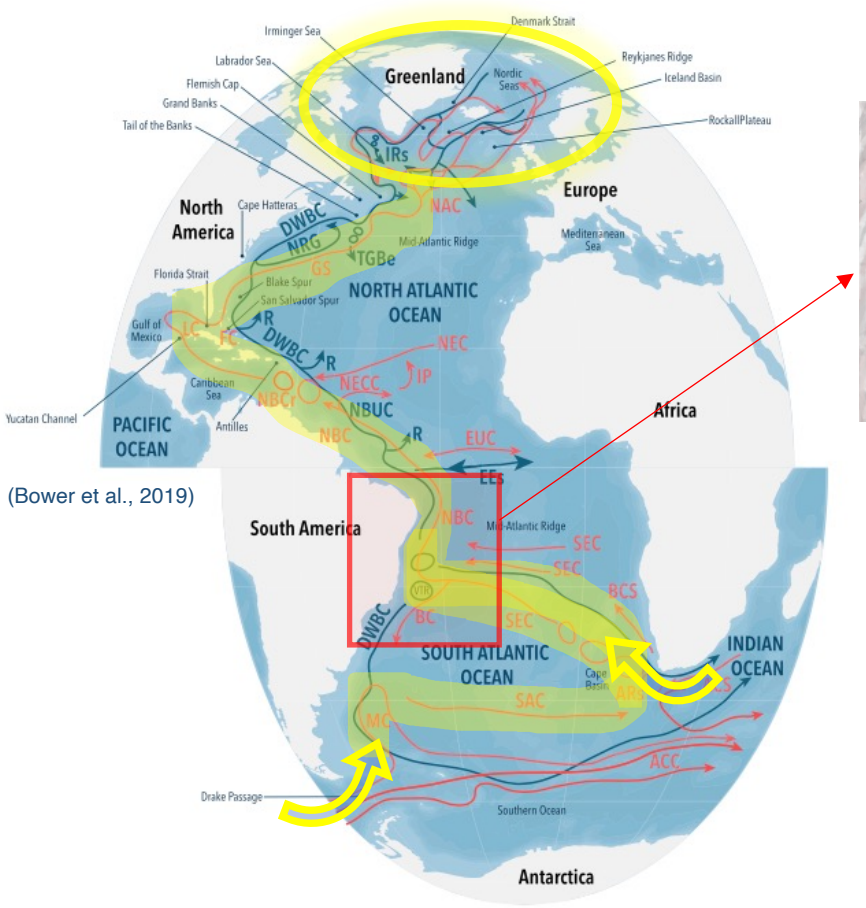


(Bower et al., 2019)

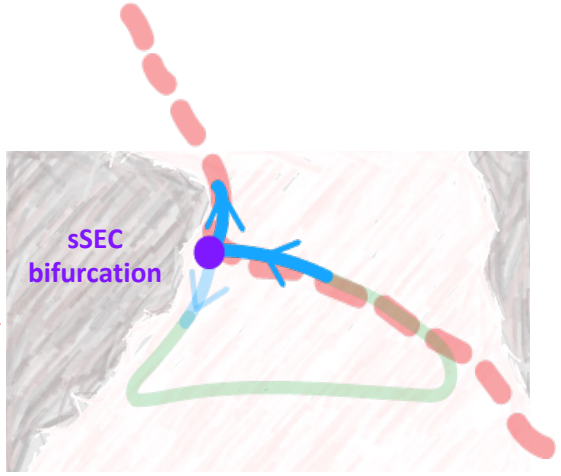


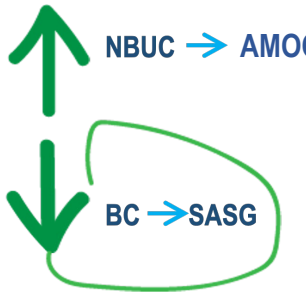


Marcello et al. (2018)
Marcello et al. (2019)

- **sSEC** = southern South Equatorial Current
- **SASG** = South Atlantic subtropical gyre
- **NBUC** = North Brazil Undercurrent
- **AMOC** = Atlantic Meridional Overturning Circulation
- **BC** = Brazil Current

## Context:

- Under human-caused global warming:
- The AMOC is expected to slow down;
- And wind-driven subtropical gyres from the Southern Hemisphere are suggested to be spinning-up and shifting southward due to large-scale atmospheric circulation changes.

- The South Atlantic is the ocean basin where the upper-ocean return flow of the AMOC (i.e., the AMOC upper limb) is primarily formed – Pacific and Indian ocean contributions are merged into the basin-wide circulation and take a ride along the SASG to be advected towards the North Atlantic to replenish deepwater formation sites.

- Therefore, the AMOC upper limb and the SASG are coupled up to the South Atlantic western boundary.
- When the sSEC bifurcates, the NBUC carries the AMOC upper limb extension northwards, and the BC closes the subtropical gyre circulation to the south.

- **If the AMOC upper limb is supposed to be weakening and the SASG circulation is supposed to be strengthening and drifting southward,**

**what is then, the resulting scenario?**

**How do wind and thermohaline forcings combine to reshape the large-scale South Atlantic circulation?**

# Weakened AMOC upper limb compensated by strengthened South Atlantic subtropical gyre in CESM1-LE simulations

- The CESM1 Large Ensemble - https://www.cesm.ucar.edu/community-projects/lens

- A single-model large ensemble – tool designed to isolate the uncertainty coming from internal variability and to therefore estimate the climate system response to external forcing, exclusively.

- And we know that the dominant factor among external forcings influencing the climate system (such as variations in solar radiation, orbital parameters and volcanic eruptions) is the rise of GHGs from burning fossil fuels to sustain humanity's modern lifestyle.

- Individual ensemble members are generated under the same external forcing conditions, and differ only in terms of random tiny perturbations in their initial condition (in their atmospheric temperature field). This is enough to ensure that each member follows a unique climate trajectory due to how energy is exchanged between all climate spheres/components (atmosphere, hydrosphere, cryosphere, lithosphere and biosphere), departing from that initial condition.

- This means that individual ensemble members differ only in terms of internal climate variability.
- The diverging trajectories of individual ensemble members generates ensemble spread – because the resulting sequences of unpredictable internal variability are randomly phased between them.
- By averaging all ensemble members and obtaining the ensemble mean, internal climate variability (i.e., the noise) is cancelled, and what is left is the response that is common to all of them: the externally-forced response – dominated by human-caused global warming.

# Weakened AMOC upper limb compensated by strengthened South Atlantic subtropical gyre in CESM1-LE simulations

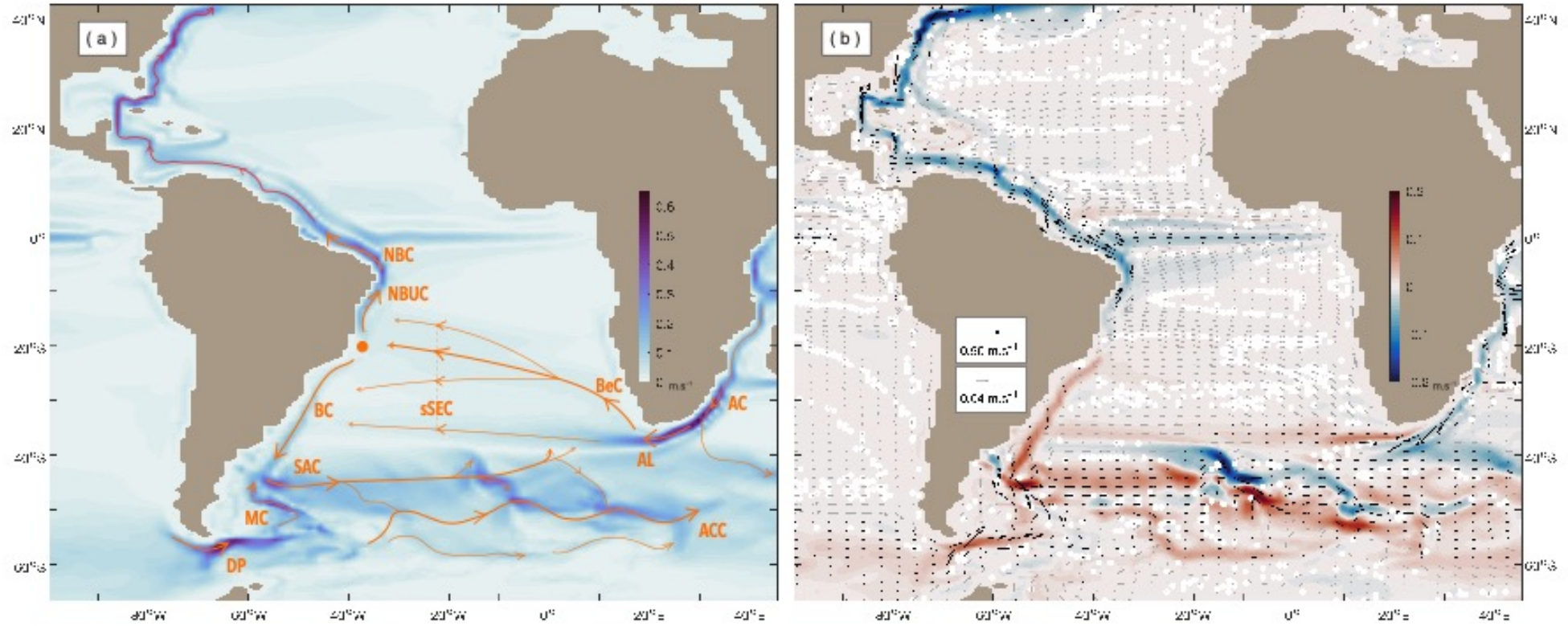


**Fig. 1 Schematic of the South Atlantic circulation and projected changes in the transport of ocean currents along the 20th and 21st centuries, as according to the ensemble mean of CESM1-LE simulations. a** Mean 1920–2100 flow field represented by the absolute magnitude of horizontal velocities averaged over the upper 985-m layer (background shading) superposed by a schematic of the South Atlantic circulation including the oceanographic features and currents mentioned in the text. DP, Drake Passage; MC, Malvinas Current; SAC, South Atlantic Current; ACC, Antarctic Circumpolar Current; AC, Agulhas Current; AL, Agulhas Leakage; BeC, Benguela Current; sSEC, southern South Equatorial Current; NBUC, North Brazil Undercurrent; NBC, North Brazil Current; BC, Brazil Current. The orange circle at ~20°S, 40°W represents the mean sSEC bifurcation latitude. **b** Ocean currents getting faster (red)/slower (blue) from 1920 to 2100. Superposing vectors denote the 1920–2100 mean horizontal velocities averaged over the upper 985-m layer, giving a perspective of the mean flow intensity and direction. The background shading represents the total trends along 1920–2100 of the absolute magnitude of upper 985 m horizontal velocity anomalies with respect to the 1920–1970 base period. Black (gray) vectors are plotted over regions where the absolute velocity magnitude is above (below) the mean value (0.035 $m.s^{-1}$), for clarity. Gray vectors are scaled by a factor of 50, in comparison with black vectors. Red (blue) indicates regions where velocity magnitudes tend to increase (decrease). Grid points where trends are not statistically significant at the 95% confidence level are marked with white dots.

# Weakened AMOC upper limb compensated by strengthened South Atlantic subtropical gyre in CESM1-LE simulations

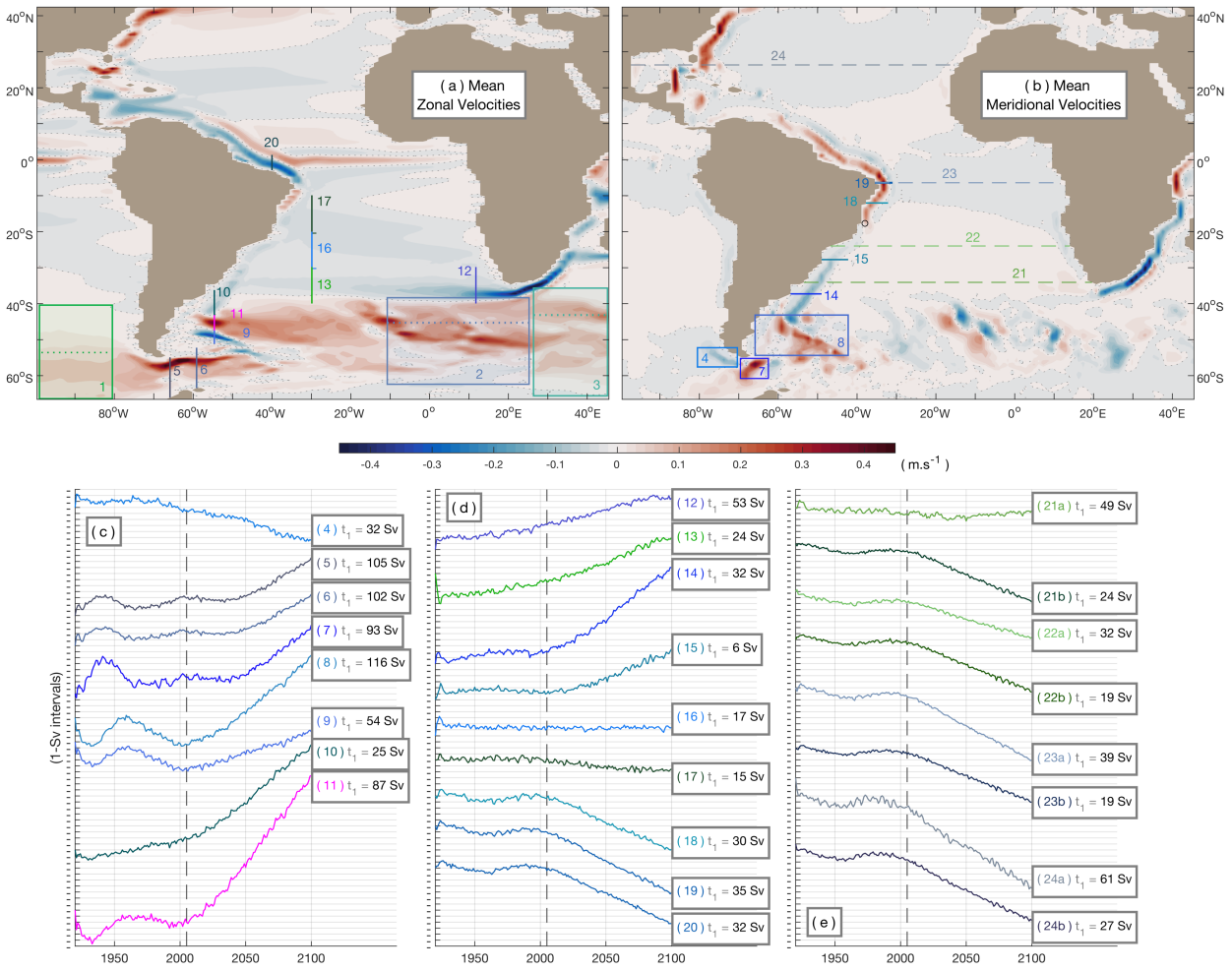


**Fig. 2 Changes in volume transports along 1920–2100.** Mean zonal (**a**) and meridional (**b**) velocity fields over 1920–2100, averaged over the upper 985-m of the ocean. In both panels, red represents positive (eastward/northward), while blue represents negative (westward/southward) velocities. Dotted gray contours indicate the zero zonal/meridional velocity line. The regions where zonal and meridional volume transports were derived are shown through boxes and transects, whose colors and numbers correspond to those on panels (**c**–**e**) and on Supplementary Fig. 1 (which shows the vertical profiles associated with boxes/transects). The volume transport time series (**c**–**e**) are integrated over the upper 985-m layer (slightly above 1-km) across transects and boxes (in the latter case, representing the mean transport along cross-sectional ranges of the boxes). Only MOC streamfunction time series (time series 21b-24b) are vertically integrated up to the depth of transition between north- and southward zonally integrated meridional velocities. When deriving eastward/northward (westward/southward) volume transports, only positive (negative) velocity values are taken into account, to avoid counterflow interference — with exception of MOC streamfunction time series (21b-24b). Panels **c**–**e** are standardized in length and their y-axis (positive upwards) varies in 1-Sverdrup intervals (1 Sv = $10^6$ $m^3.s^{-1}$). The legends indicate the value corresponding to the first time-step (year of 1920) in each time series ($t_1$). The gray dashed vertical line marks the transition from the historical (1920–2005) to the RCP8.5 (2006–2100) period. Time series mean and trend values are displayed in Supplementary Table 1.

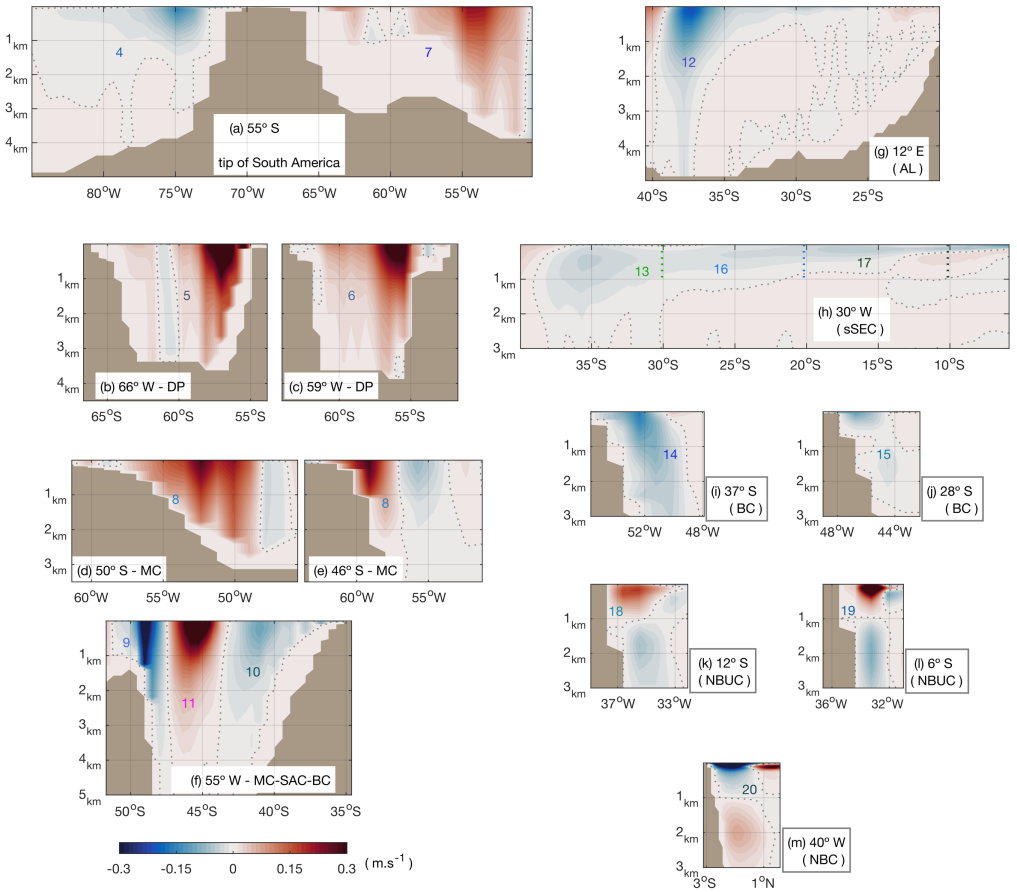


Supplementary Figure 1: | **Vertical profiles corresponding to boxes/transects and volume transport time series in article Figure 2** |. 1920-2100 mean meridional (**a**, **d**, **e**, **i**, **j**, **k**, **l**) and zonal (**b**, **c**, **f**, **g**, **m**) velocities. Red represents positive (eastward/northward), while blue represents negative (westward/southward) velocities. Dotted gray contours indicate the zero zonal/meridional velocity line. The x- and y-axis ranges of all profiles are scaled, matching each other, in order to provide a perspective of relative flow width and depth. The volume transport time series in article Figure 2 are integrated in the upper 985-m layer (slightly above 1-km), where the strongest core of surface ocean currents are located – deeper layers are shown to provide a vertical perspective of their distribution. Eastward/northward (westward/southward) volume transports in article Figure 2 were derived by taking into account only positive/red (negative/blue) velocity values to avoid counterflow interference. DP = Drake Passage, MC = Malvinas Current, SAC = South Atlantic Current, BC = Brazil Current, AL = Agulhas Leakage, sSEC = southern branch of the South Equatorial Current, NBUC = North Brazil Undercurrent, NBC = North Brazil Current.

# Weakened AMOC upper limb compensated by strengthened South Atlantic subtropical gyre in CESM1-LE simulations

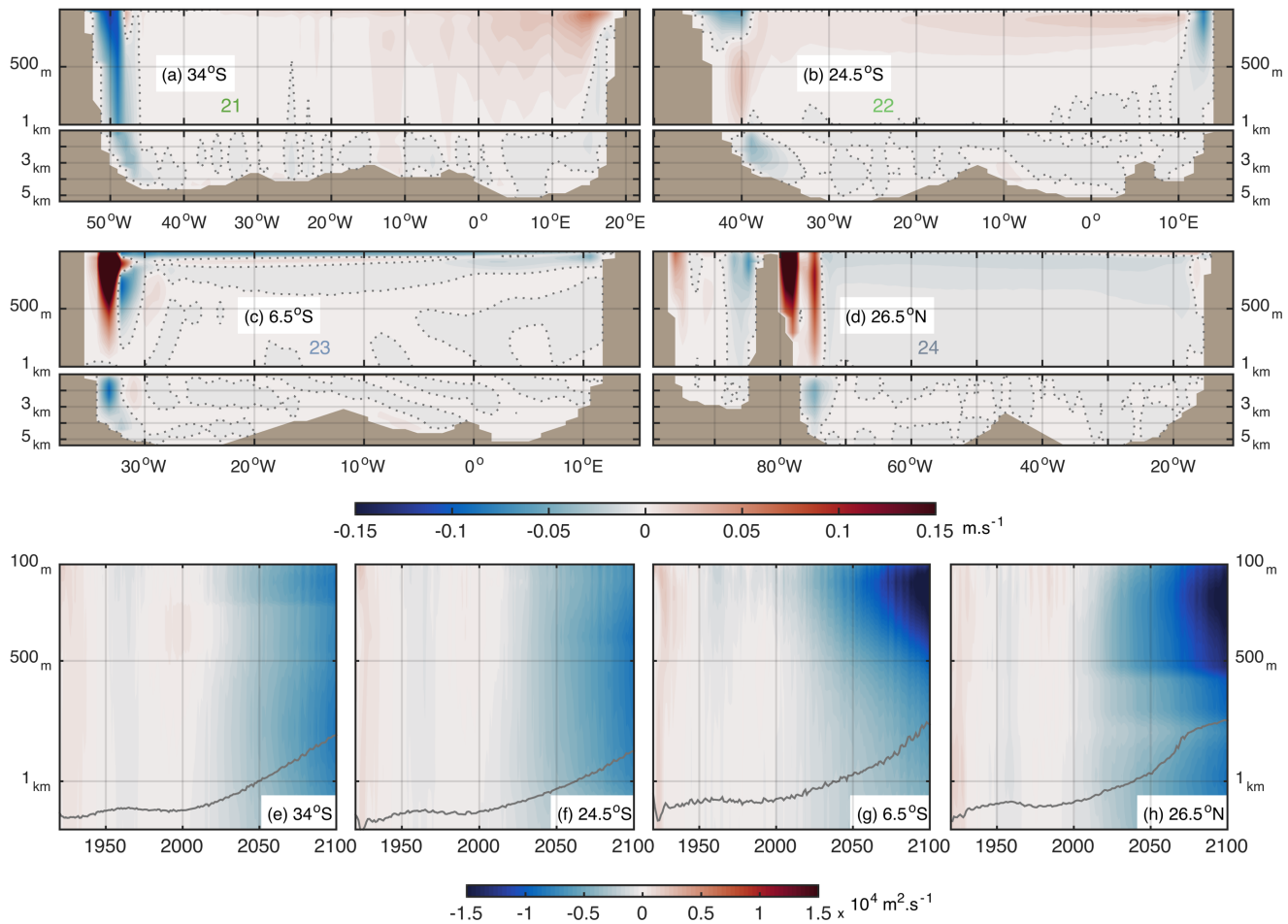


**Fig. 3 Projected weakening of the AMOC upper limb from 34°S to 26.5°N. a–d** Transbasin meridional velocity profiles (1920–2100 mean) at 34°S, 24.5°S, 6.5°S and 26.5°N, respectively. Red (blue) represents mean northward (southward) velocities. **e–h** Hovmoller diagrams of zonally integrated meridional velocity anomalies along transbasin sections corresponding to **a–d**. Blue (red) represents negative/southward (positive/northward) anomalies. The gray filled contour marks the 1920–2100 evolution of the zero meridional velocity line that delimits the lower limit of the AMOC upper limb. The upper 100-m of Hovmoller diagrams are not shown since it reflects near-surface dynamics within the Ekman layer, which are out of our scope.

# Weakened AMOC upper limb compensated by strengthened South Atlantic subtropical gyre in CESM1-LE simulations

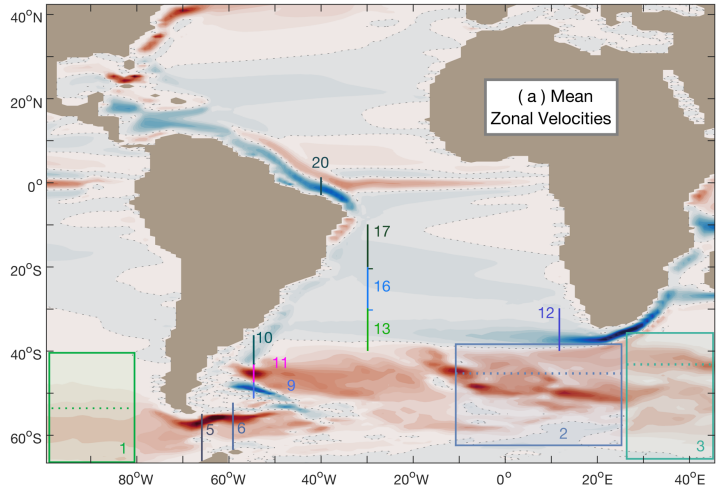


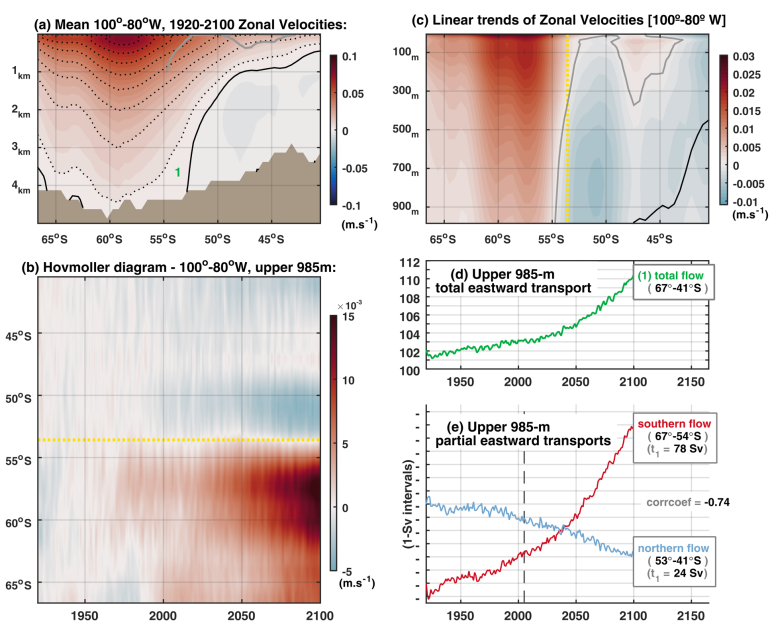


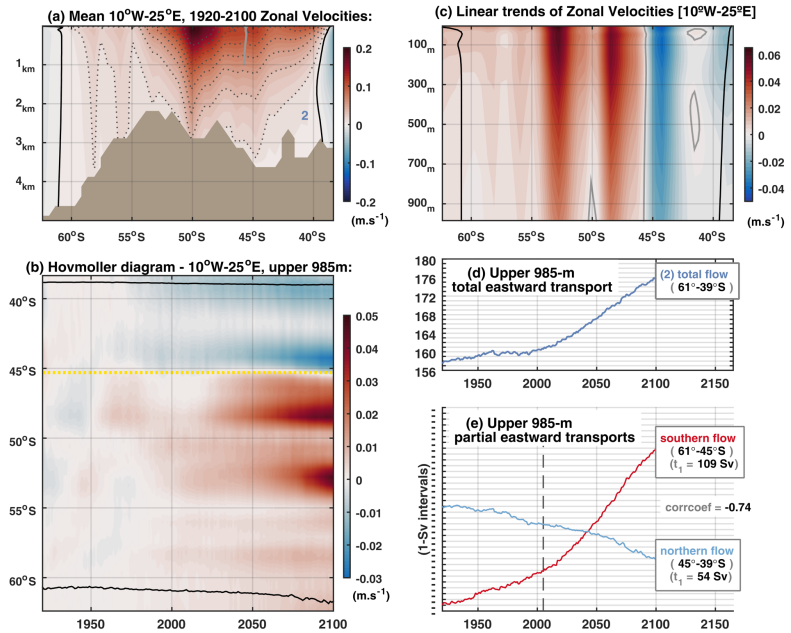


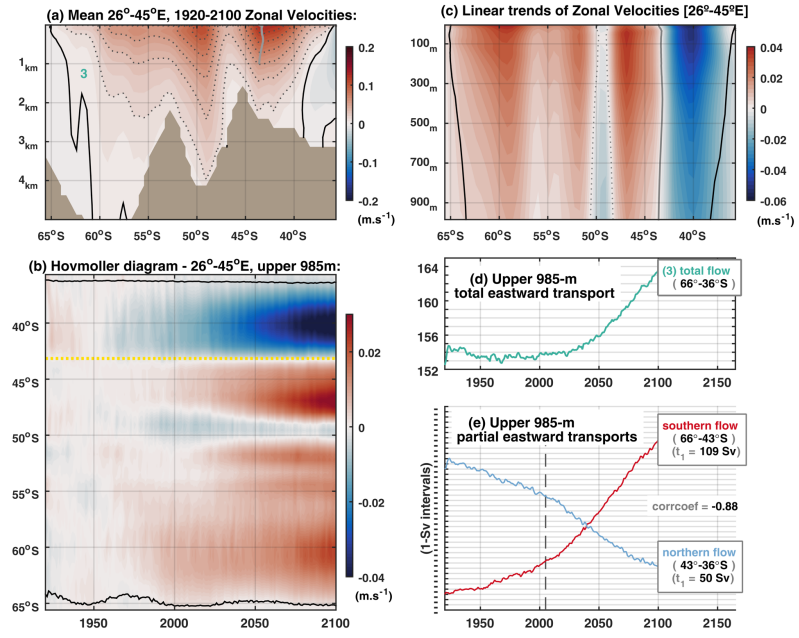


- Figures S2, S3, S4.

# Weakened AMOC upper limb compensated by strengthened South Atlantic subtropical gyre in CESM1-LE simulations

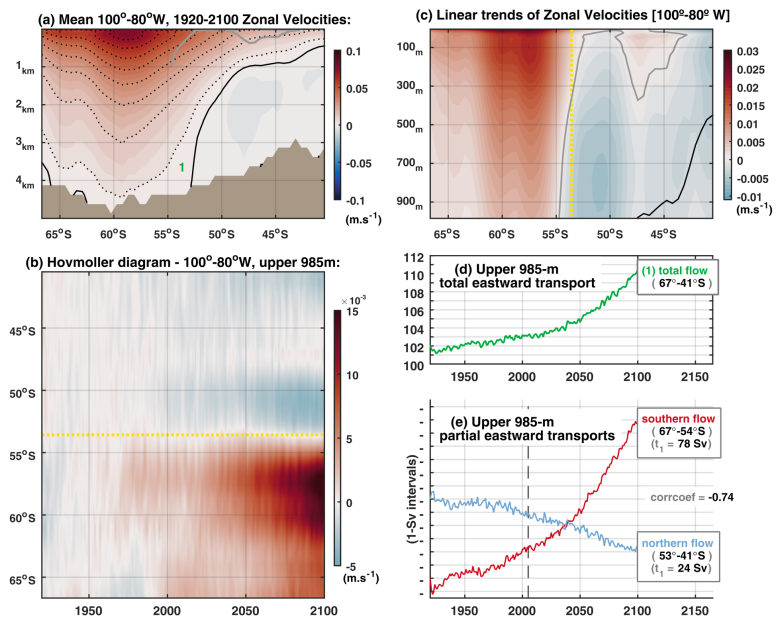


Supplementary Figure 2: | **Southern eastward flows prior to the Drake Passage (100°-80°W)** | Zonal velocities in the southern Pacific sector, averaged over 100°-80°W (box number 1 in article Figure 2a). (**a**) 1920-2100 mean vertical profile; red denotes positive (eastward) and blue denotes negative (westward) velocities. The black filled contour represents the zero zonal velocity line; and the black dotted contours indicate zonal velocity lines along contour intervals of $4x10^{-3}$:$10^{-2}$:$74x10^{-3}$. The gray filled contour in the upper 1-km is reproduced from (c), for reference. (**b**) Hovmoller diagram (upper 985-m mean) of anomalous zonal velocities (1920-1970 base period); red (blue) indicates positive/eastward (negative/westward) anomalies. The yellow dotted line marks the mean latitude of transition between positive and negative anomalies (53.5°S), in correspondence to the yellow dotted line in (c), used as a reference to derive the southern and northern volume transports in (e). (**c**) 1920-2100 total trends of anomalous zonal velocities, corresponding to the upper 985-m layer in (a). The gray filled contour marks the transition from negative (blue) to positive (red) trends. The black filled contour corresponds to the upper 985-m portion of the black contour in (a), indicating where the mean flow shifts from eastward to westward velocities. (**d**) Time series of the total eastward volume transport associated with the upper 985-m of the zonal velocities in (a), along 67°-41°S. (**e**) Time series of the southern and northern portions of the total eastward transport in (d). The value corresponding to their first time step (1920) is indicated, while the y-axis varies in 1-Sverdrup intervals (1 Sv = $10^6$ $m^3.s^{-1}$). The gray dashed vertical line indicates the transition from the historical (1920-2005) to the RCP8.5 (2006-2100) period. The correlation coefficient between both detrended, standardized time series is indicated (-0.74).

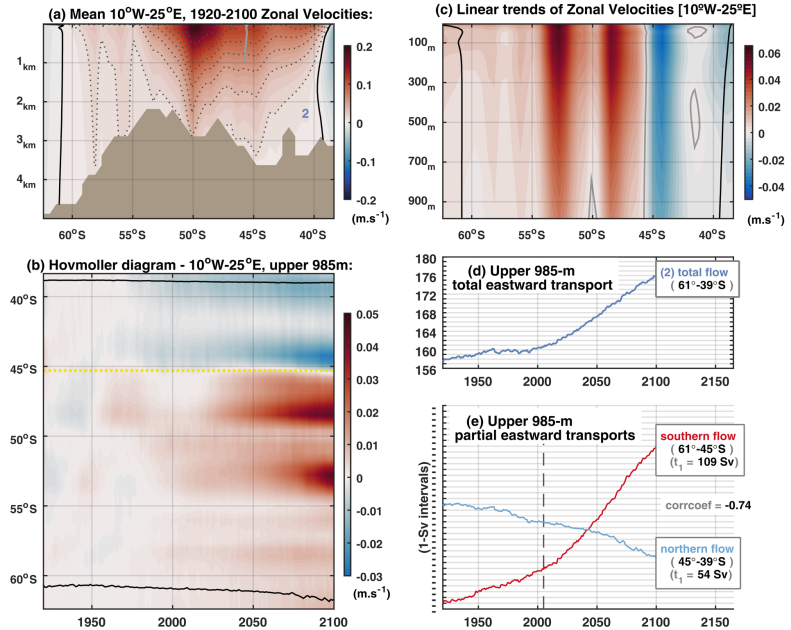


Supplementary Figure 3: | **Southern eastward flows throughout the eastern South Atlantic sector (10°W-25°E)** | Zonal velocities in the southeastern Atlantic sector, averaged over 10°W-25°E (box number 2 in article Figure 2a). (**a**) 1920-2100 mean vertical profile; red denotes positive (eastward) and blue denotes negative (westward) velocities. The black filled contour represents the zero zonal velocity line; and the black dotted contours indicate zonal velocity lines along contour intervals of $14x10^{-3}$:$2x10^{-2}$:$154x10^{-3}$. The gray filled contour in the upper 1-km is reproduced from (c), for reference. (**b**) Hovmoller diagram (upper 985-m mean) of anomalous zonal velocities (1920-1970 base period); red (blue) indicates positive/eastward (negative/westward) anomalies. The black contour represents the temporal evolution of the mean zero zonal velocity line corresponding to the upper 985-m average in (a). The yellow dotted line marks the mean latitude of transition between positive and negative anomalies (45.3°S), in correspondence to the full-depth gray contour in (c) along this latitude, used as a reference to derive the southern and northern volume transports in (e). (**c**) 1920-2100 total trends of anomalous zonal velocities, corresponding to the upper 985-m layer in (a). The gray filled contour marks the transition from negative (blue) to positive (red) trends. The black filled contour corresponds to the upper 985-m portion of the black contour in (a), indicating where the mean flow shifts from eastward to westward velocities. (**d**) Time series of the total eastward volume transport associated with the upper 985-m of the zonal velocities in (a), along 61°-39°S. (**e**) Time series of the southern and northern portions of the total eastward transport in (d). The value corresponding to their first time step (1920) is indicated, while the y-axis varies in 1-Sverdrup intervals (1 Sv = $10^6$ $m^3.s^{-1}$). The gray dashed vertical line indicates the transition from the historical (1920-2005) to the RCP8.5 (2006-2100) period. The correlation coefficient between both detrended, standardized time series is indicated (-0.74).

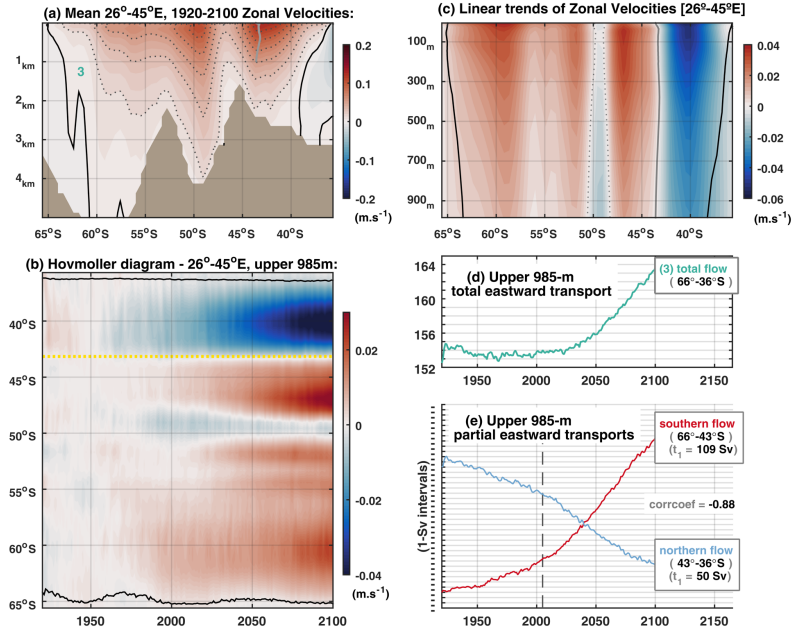


Supplementary Figure 4: | **Southern eastward flows entering the Indian Ocean sector (26°-45°E)** | Zonal velocities of the ocean currents leaving the Atlantic towards the Indian basin, averaged over 26°-45°E (box number 3 in article Figure 2a). (**a**) 1920-2100 mean vertical profile; red denotes positive (eastward) and blue denotes negative (westward) velocities. The black filled contour represents the zero zonal velocity line; and the black dotted contours indicate zonal velocity lines along contour intervals of $14x10^{-3}$:$2x10^{-2}$:$154x10^{-3}$. The gray filled contour in the upper 1-km is reproduced from (c), for reference. (**b**) Hovmoller diagram (upper 985-m mean) of anomalous zonal velocities (1920-1970 base period); red (blue) indicates positive/eastward (negative/westward) anomalies. The black contour represents the temporal evolution of the mean zero zonal velocity line corresponding to the upper 985-m average in (a). The yellow dotted line marks the mean latitude of transition between positive and negative anomalies (43.2°S), in correspondence to the full-depth gray contour in (c) along this latitude, used as a reference to derive the southern and northern volume transports in (e). (**c**) 1920-2100 total trends of anomalous zonal velocities, corresponding to the upper 985-m layer in (a). The gray filled contour marks the transition from negative (blue) to positive (red) trends. The black filled contour corresponds to the upper 985-m portion of the black contour in (a), indicating where the mean flow shifts from eastward to westward velocities. (**d**) Time series of the total eastward volume transport associated with the upper 985-m of the zonal velocities in (a), along 66°-36°S. (**e**) Time series of the southern and northern portions of the total eastward transport in (d). The value corresponding to their first time step (1920) is indicated, while the y-axis varies in 1-Sverdrup intervals (1 Sv = $10^6$ $m^3.s^{-1}$). The gray dashed vertical line indicates the transition from the historical (1920-2005) to the RCP8.5 (2006-2100) period. The correlation coefficient between both detrended, standardized time series is indicated (-0.88).

# Weakened AMOC upper limb compensated by strengthened South Atlantic subtropical gyre in CESM1-LE simulations

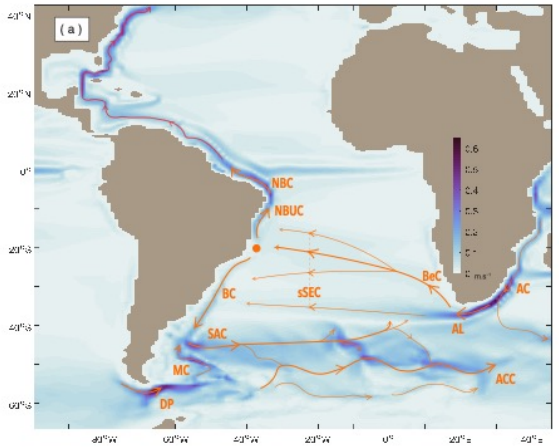


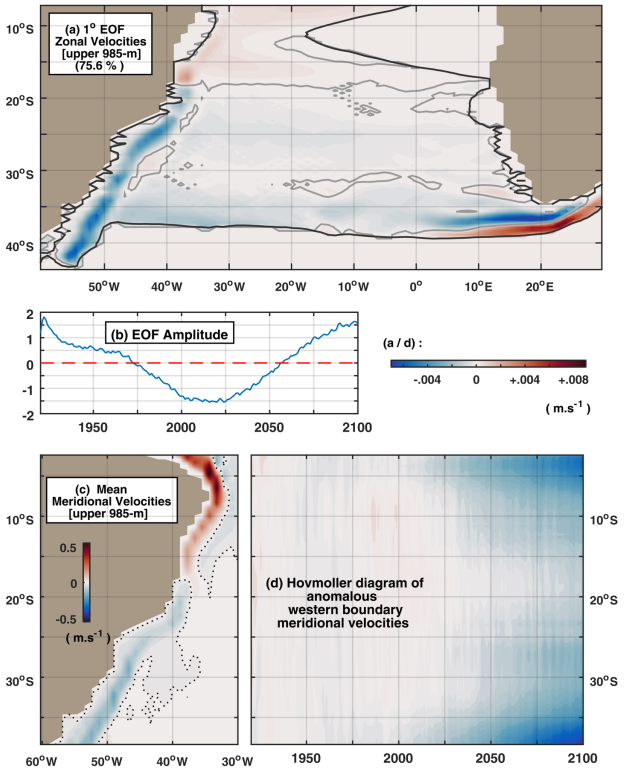


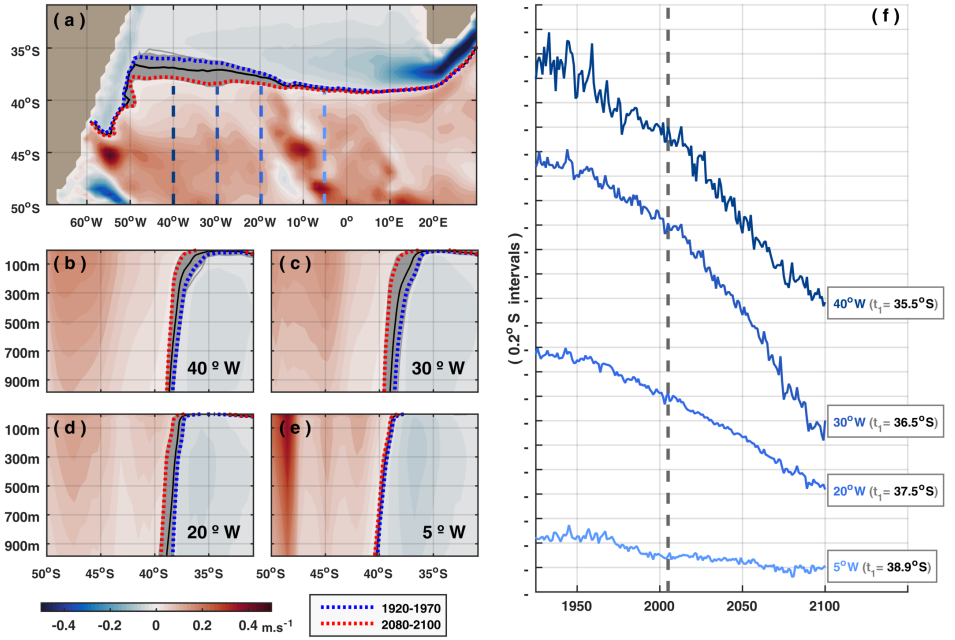


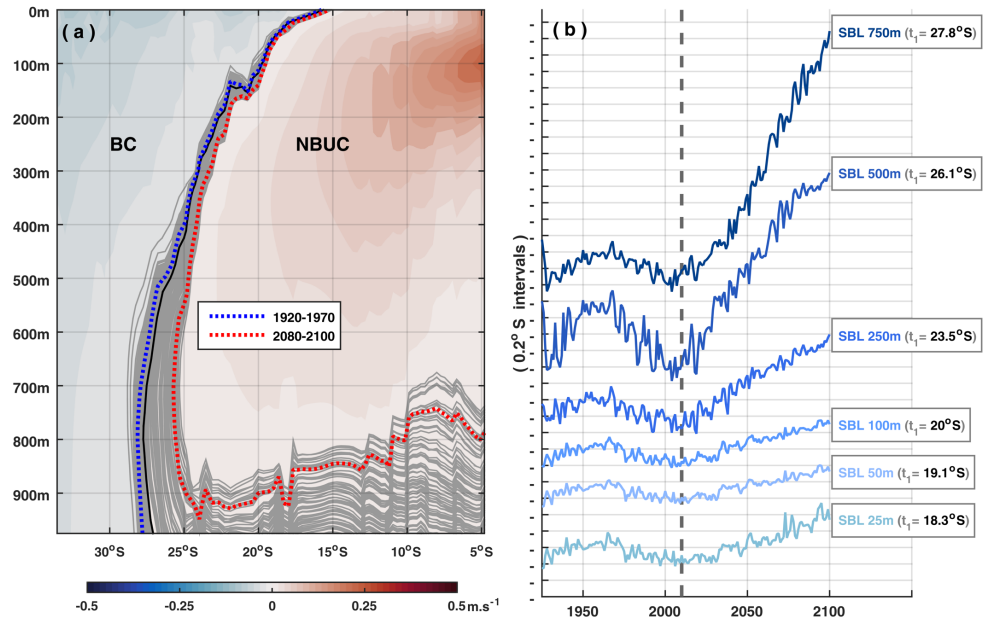

# Weakened AMOC upper limb compensated by strengthened South Atlantic subtropical gyre in CESM1-LE simulations

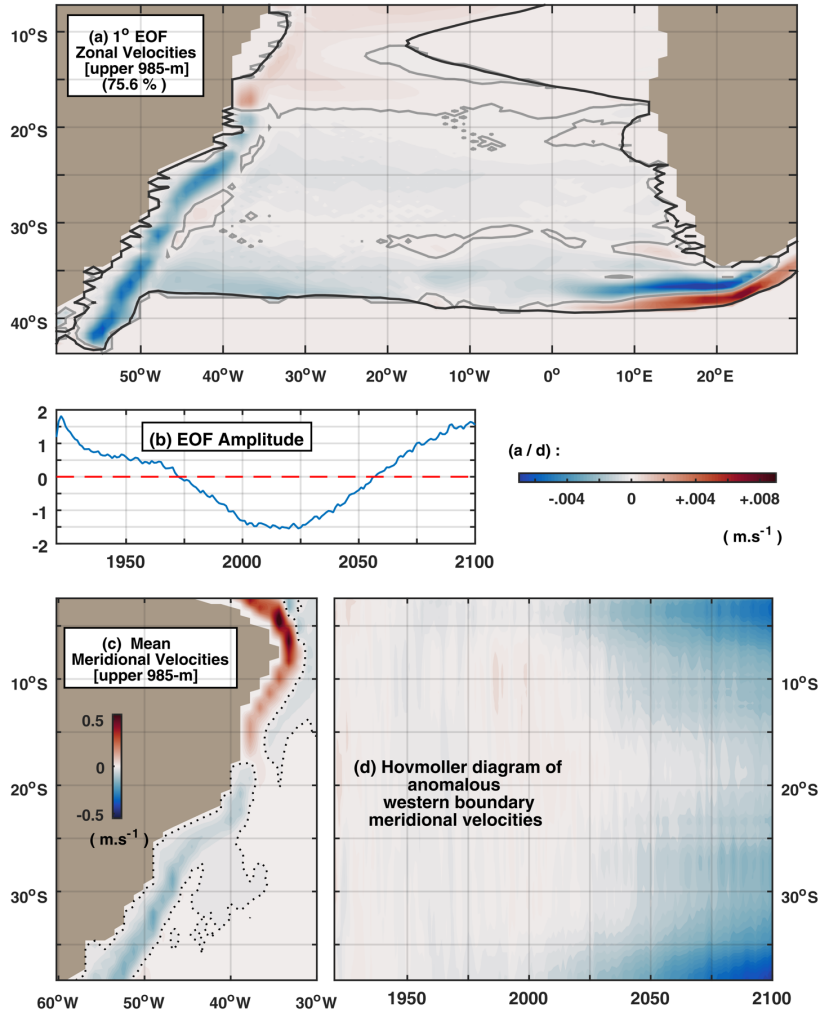


**Fig. 4 Changes in the distribution of zonal and meridional SASG flows. a** Spatial pattern of the leading EOF (94.9% of total variance) of zonal velocity anomalies along 1920–2100 within the upper 985-m of the South Atlantic subtropical gyre (delimited by the 1920–2100 mean zero zonal velocity line — black filled contour). Trends were not removed from the data prior to performing the EOF. **b** Corresponding dimensionless amplitude, or Principal Component (PC), time series (blue) and its linear trend along 1920–2100 (red dashed line). **c** 1920–2100 mean, upper 985-m, meridional velocities along the SA western boundary, showing the north-south distribution of the WBCs, for reference. **d** Hovmoller diagram of anomalous meridional velocities averaged over the western boundary layer (within a 6°-longitude band off the South American coast), corresponding to the meridional extension in **c**.

# Weakened AMOC upper limb compensated by strengthened South Atlantic subtropical gyre in CESM1-LE simulations

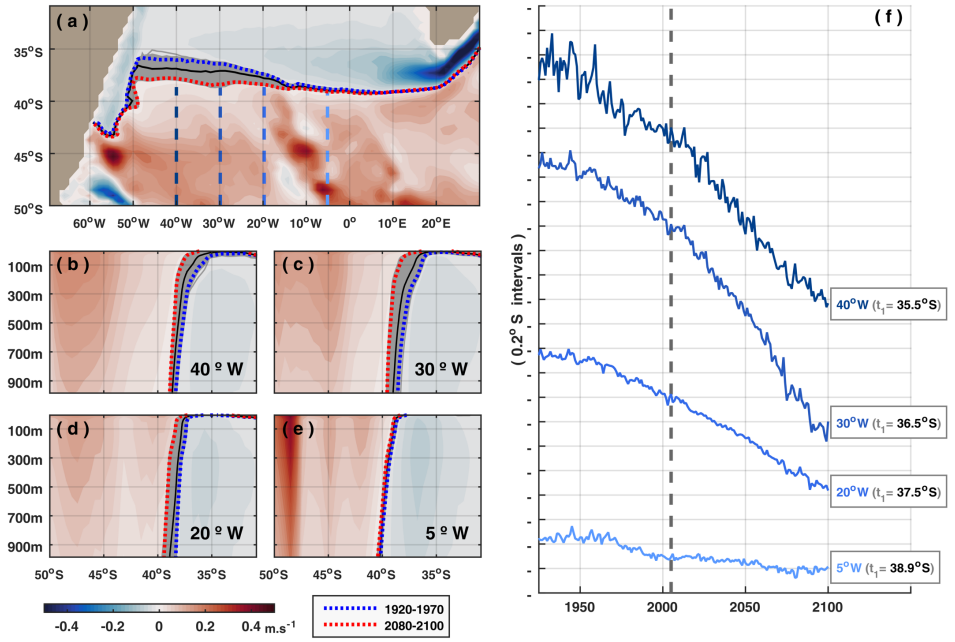


**Fig. 5 Poleward shift of the western SASG center.** 1920–2100 mean zonal velocities (background colors): (**a**) at the zonal-meridional plane, averaged over the upper 985-m; **b**–**e** and along depth at 40°W, 30°W, 20°W and 5°W, respectively. **a**–**e** The mean zero zonal velocity line is shown for: 1920–2100 (black filled contour), 1920–1970 (blue dotted contour) and 2080–2100 (red dotted contour); gray filled contours show its annual evolution along 1920–2100. Vertical dashed lines in **a** correspond to the locations where vertical profiles are shown in **b**–**e** as well as to where time series of the zero zonal velocity line were derived at 100-m depth – shown in **f**. The value corresponding to the first time step (1920) of each time series is indicated, while the y-axis varies in 0.2°-latitude intervals (increasing from south to north, thus sign convention is negative downwards for a southward migration of the zero zonal velocity line). The gray dashed vertical line indicates the transition from the historical (1920–2005) to the RCP8.5 (2006–2100) period.

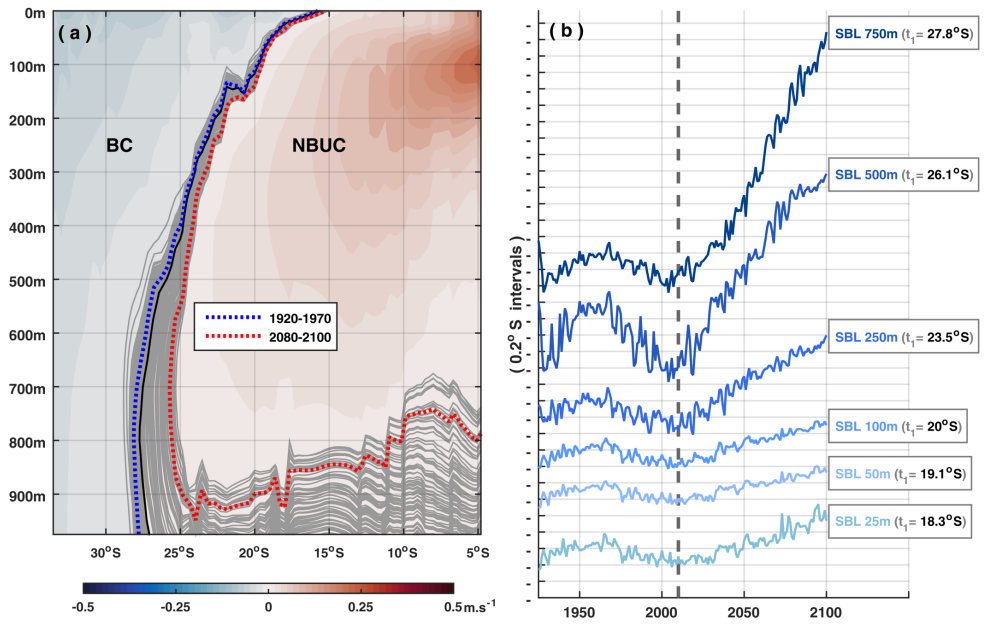


**Fig. 6 Equatorward shift of the sSEC bifurcation latitude at the SASG northwestern boundary. a** 1920–2100 mean meridional velocities averaged over the western boundary layer (<4° from the South American coast). Positive (negative) values indicate northward (southward) flows associated with the NBUC (BC). The bifurcation of the sSEC is represented by the zero meridional velocity line, shown for the mean periods of 1920–2100 (black filled contour), 1920–1970 (blue dotted contour) and 2080–2100 (red dotted contour); gray filled contours show its annual evolution along 1920–2100. **b** Time series of the sSEC bifurcation latitude at different depths. The value corresponding to the first time step (1920) of each time series is indicated, while the y-axis varies in 0.2°-latitude intervals (increasing from south to north, thus sign convention is positive upwards for a northward migration of the SBL). The gray dashed vertical line indicates the transition from the historical (1920–2005) to the RCP8.5 (2006–2100) period.

# Weakened AMOC upper limb compensated by strengthened South Atlantic subtropical gyre in CESM1-LE simulations

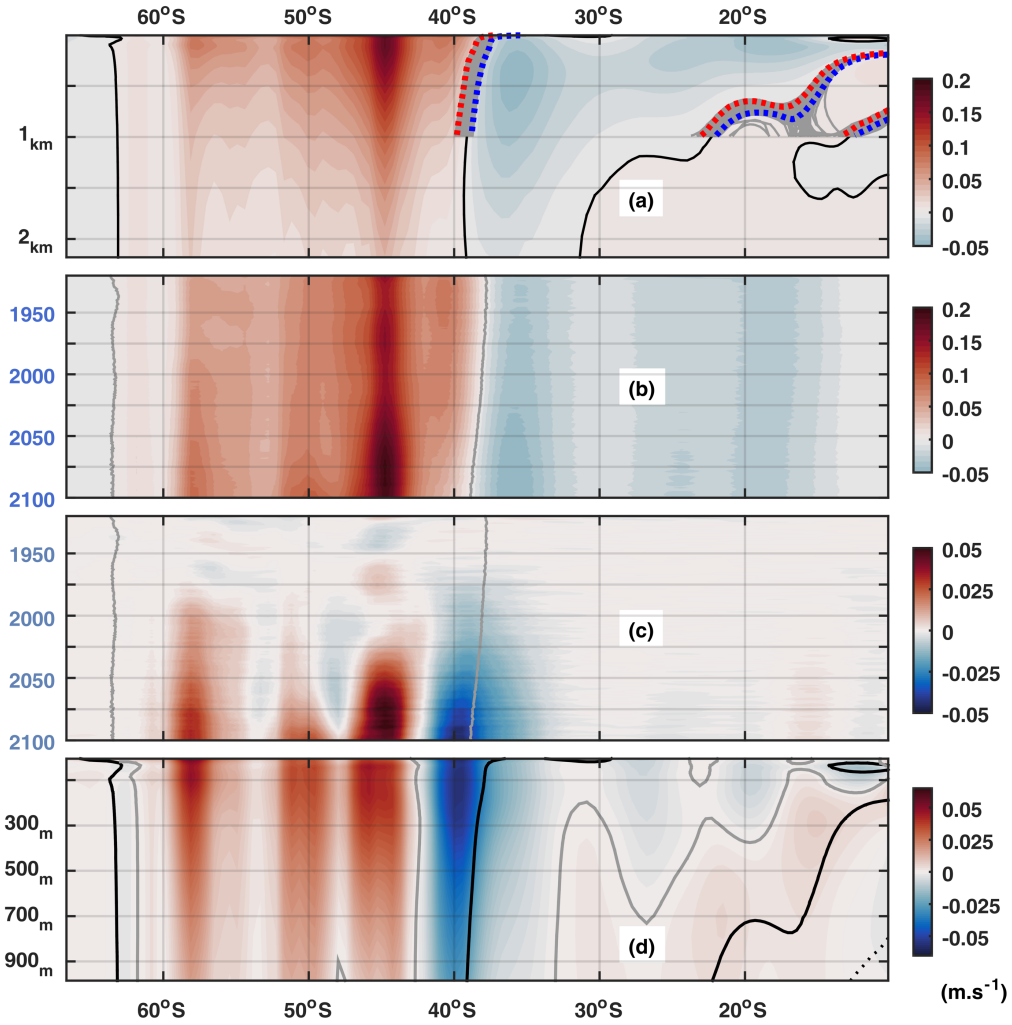


Supplementary Figure 5: | **SASG structural changes (30°-10°W)** | Climatological (1920-2100 mean) and anomalous (with respect to the 1920-1970 base period) zonal velocities (m.s$^{-1}$) centered at the South Atlantic subtropical gyre (SASG) (30°-10°W zonal average): (**a**) Climatological vertical profile (Latitude x Depth), depicting the westward flow of the consecutive sSEC branches at the northern limb of the subtropical gyre (blue) and the eastward SAC flow at the southern limb of the subtropical gyre merged with the ACC flow in the Southern Ocean (red). Black contours mark the climatological zero zonal velocity line, whose upper 985-m, 1920-2100 annual evolution is represented by gray contours (filling the whole range of their southward migration since 1920), delimited by the 1920-1970 (blue dotted contours) and 2080-2100 (red dotted contours) climatologies. (**b**, **c**) Hovmoller diagrams of the upper 985-m average of raw (b) and anomalous (c) zonal velocities; red (blue) denotes positive/eastward (negative/westward) raw velocity values (b) / anomalous velocity values (c); the gray thick line in (b) (also reproduced in (c), for reference) marks the temporal evolution of the zero zonal velocity line averaged over the upper 985-m; (**d**) 1920-2100 total trends of anomalous zonal velocities corresponding to the upper 985-m in (a). The black thick contour is reproduced from (a), for reference, corresponding to the upper 985-m mean zero zonal velocity line that separates west- from eastward mean flows. The gray filled contour separates positive from negative trends over 1920-2100. Red (blue) denotes positive (negative) trends, i.e., regions where eastward (westward) anomalies tend to increase.

## 6. Supplementary Description of Figure S5:

The sSEC system is entirely displaced southward (Figure S5a). The temporal evolution of raw (Figure S5b) and anomalous (Figure S5c) zonal velocities averaged over the upper 985-m evidences the strengthening of the sSEC at its southernmost portion, while the SAC actually weakens near the zero zonal velocity line setting its northern limit, and strengthens south of ~42°S. Consistent anomalies start developing past ~2000s (Figure S5c).

In Figure 5d, the 1920-2100 trends of the anomalous zonal velocities corresponding to the upper 985 m of Figure S5a reveal a more comprehensive perspective of changes in the sSEC structure along the meridional-depth plane: showing that projected anomalies in the sSEC system are split meridionally between two counterparts in a convoluted bowl-shaped way along depth – with a weakened (strengthened) northern (southern) counterpart, depicted by the red, eastward (blue, westward) anomalies.

This clarifies why the upper 985 m vertically integrated volume transports of the southern, central and northern sSEC (shown in Figure S1h) display increasing, nearly-zero and decreasing long-term trends, respectively (article Figure 2, time series 13, 16 and 17). These transports account only for the westward velocities corresponding to the sSEC system (blue shading in between black contours in Figure S5a); and while the southern sSEC range (30°-40°S) encompasses mostly negative (i.e., westward-strengthening) anomalies, the central sSEC range (20°-30°S) encompasses both negative and positive anomalies along depth in similar proportions – suggesting they cancel each other producing neither a westward strengthening nor weakening; and the northern sSEC range (10°-20°S) encompasses mostly positive (eastward, weakening) anomalies.

In summary, the westward transport along the northern boundary of the SASG (i.e., the sSEC) is slowing down along outer, northern portions while speeding up along inner, southern portions.

# Weakened AMOC upper limb compensated by strengthened South Atlantic subtropical gyre in CESM1-LE simulations

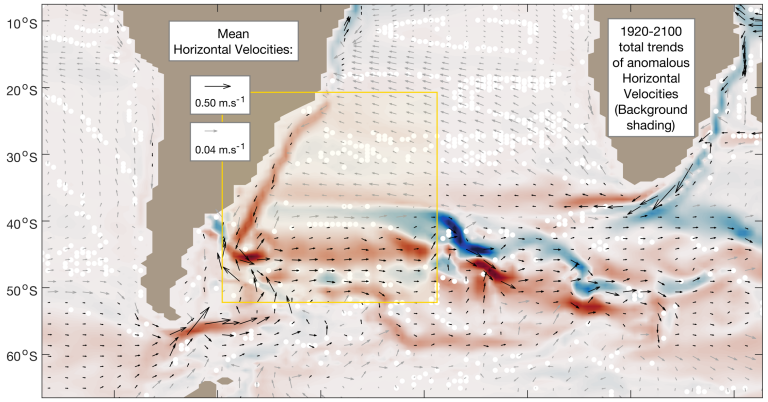


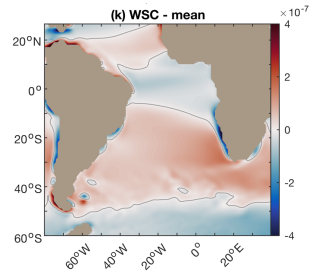


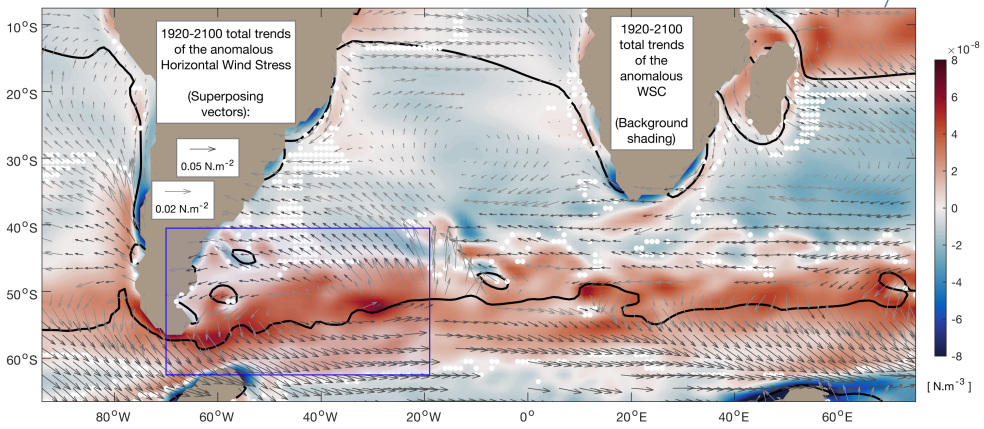


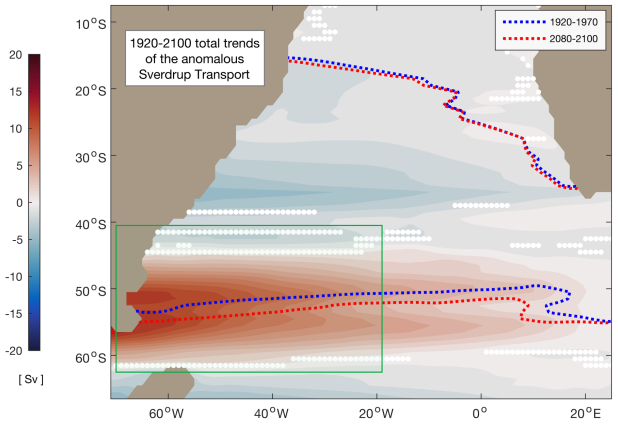


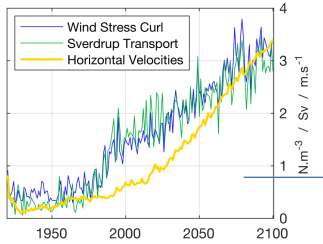


The Sverdrup balance implies an intensification of the SASG basin interior transport at its southern portion along with a poleward expansion of the gyre over the whole zonal extension of the basin.

More specifically, the SASG interior is projected to spin-down between ~15◦–45◦S and to spin-up south of that, as a result of the local WSC anomalies. Though note that Sverdrup dynamics prevail only far from the western boundary[139], and therefore do not directly illustrate the strengthening of the BC (happening from 20◦S downstream); which is, according to this theory, indirectly represented by the compensating northward transport in the basin interior.

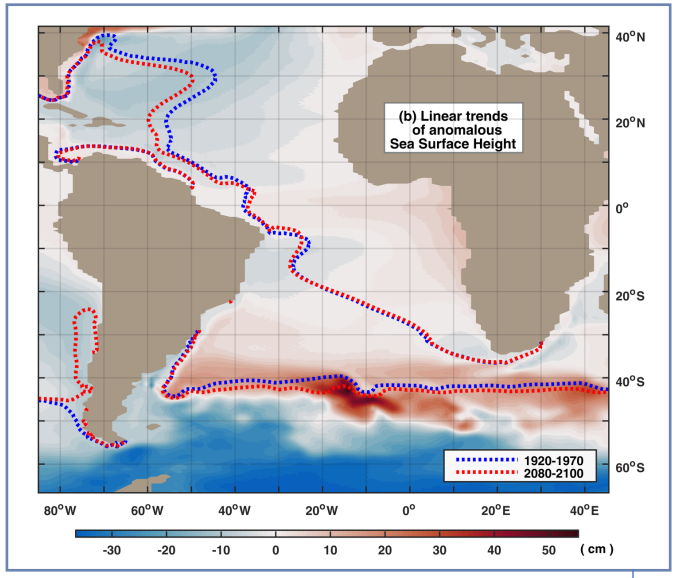


However, the degree to which the real SASG interior transport is in Sverdrup balance might be compromised by density-driven changes in the AMOC and by the inflow of interocean waters with distinct physical properties.

Overturning and gyre circulations are fundamentally linked[140], and the SA is especially sensitive to both low-frequency buoyancy-forced variations due to perturbed AMOC dynamics and wind-forced changes[102]. It is far out of our scope to categorically investigate the reasons for a projected AMOC slow-down, still, changes in high-latitude AMOC forcing are expected to call for compensating effects involving upstream surface AMOC pathways[28–30]. As the AMOC weakens, it changes the meridional transport along the whole extension of the AMOC upper limb, including the subtropical oceans — hence potentially compromising the extent to which the wind field determines the flow in the ocean interior[141]. And this is particularly meaningful for the SA — where the AMOC upper limb travels precisely along the subtropical gyre interior, which is the target region described by the Sverdrup theory. Therefore, interbasin transfers[142] and flow compensations as adjustments to changes in overturning might partially offset the changes induced by the shifted wind pattern via Sverdrup dynamics.

Moreover, the climatological wind-driven BC is known to be weak among global WBCs, since the larger portion of the sSEC normally forms the NBUC along the AMOC upper limb[129,143]. In a warming climate with a declining AMOC, the opposite holds true: as the NBUC weakens, the sSEC then feeds the BC to a larger extent. Since the mean BC transport is not well explained only by surface wind variations, the same is expected for changes in its projected transport[98].

Overall, the WSC and Sverdrup transport change patterns are consistent with the notion of a southwestward strengthening of the SASG, where the positive anomalies of the WSC and of the horizontal velocities' absolute magnitude are correlated at r = 0.52

Finally, as wind anomalies act to pile up waters at the western and southern portions of the SASG, the sea level tends to rise over these regions. That is because spatially varying SSH trends reflect the geographical redistribution of upper-ocean water masses[68,70,92,144–146]. In the mean climatology (Supplementary Fig. 8), wind-driven convergence forms a SSH hill at the SASG center, with its anticyclonic geostrophic circulation revolving around a maximum SSH. Under future climate change, the SASG center is displaced poleward, while the sea level tends to drop over its weakened northern boundary.

# Weakened AMOC upper limb compensated by strengthened South Atlantic subtropical gyre in CESM1-LE simulations

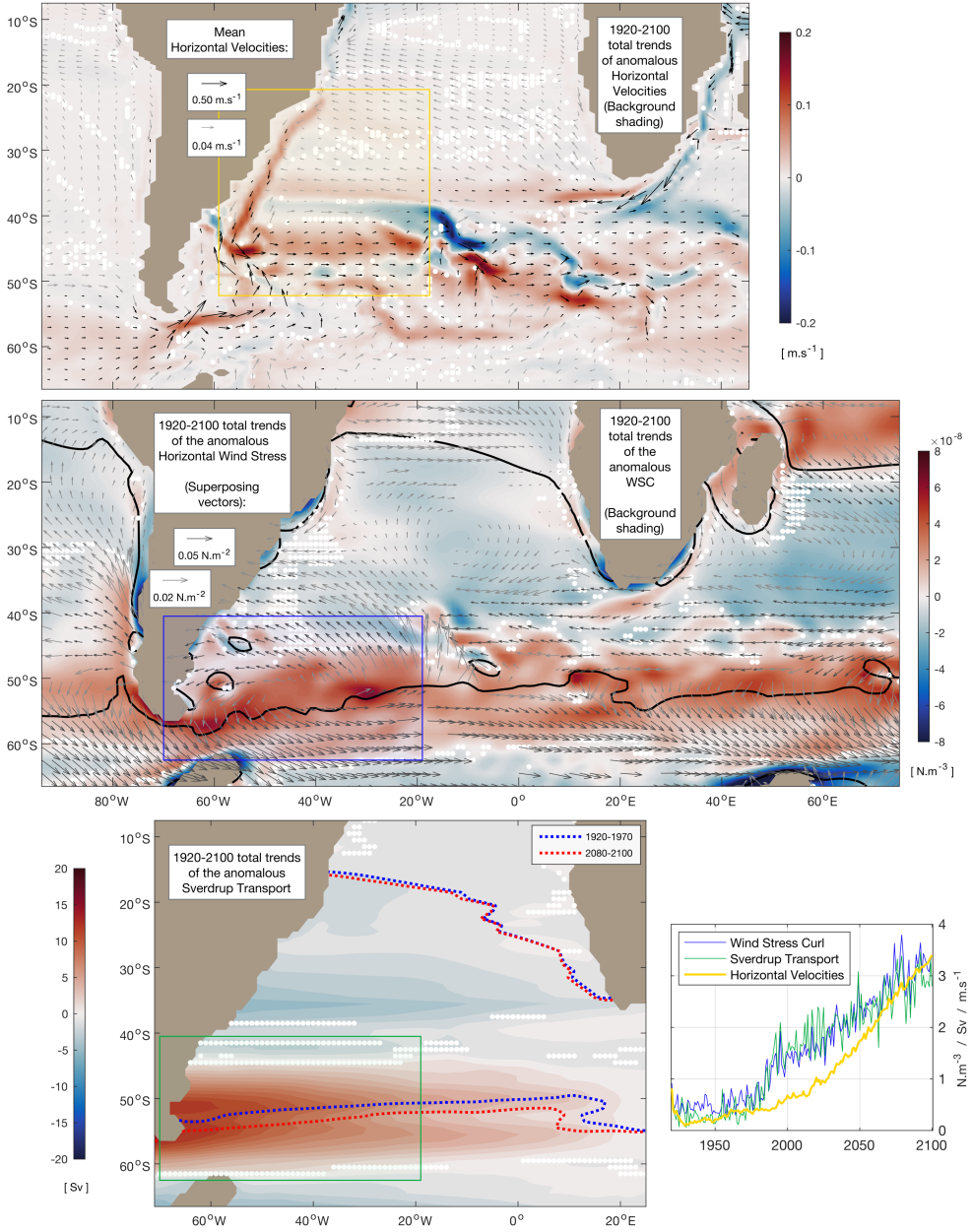


Supplementary Figure 6: | **Wind pattern changes** | Trends along 1920-2100 with respect to the 1920-1970 base period. **(a)** Same as Figure 1 from the article, with focus on the South Atlantic, to aid visual interpretation. Superposing vectors denote the mean flow field while the background shading indicates the regions where ocean currents tend to strengthen (red) or weaken (blue). Please refer to article Figure 1 caption for further details. **(b)** Wind stress (superposing vectors) and wind stress curl (background shading) trends. Black (gray) vectors are plotted over regions where the horizontal wind stress magnitude is above (below) the 0.014 $N.m^{-2}$ value, to aid visual presentation. The black contour represents the climatological zero wind stress curl line, which delimits the positive, anticyclonic wind stress curl at subtropical regions. **(c)** Sverdrup transport trends (1 Sv = $10^6$ $m^3.s^{-1}$). The red (blue) dotted contour represents the mean 1920-1970 (2080-2100) zonally integrated zero wind stress curl line. Only statistically significant wind stress trend vectors are plotted, while points where wind stress curl trends (and also Sverdrup transport trends in **c**) are non-statistically significant are indicated by the white dots (the 95% confidence level was adopted). **(d)** Standardized time series of the mean positive anomalies of the absolute magnitude of horizontal velocities, of the wind stress curl and of the Sverdrup transport, averaged over the regions indicated by the yellow (a), blue (b) and green (c) boxes, respectively.

# Weakened AMOC upper limb compensated by strengthened South Atlantic subtropical gyre in CESM1-LE simulations

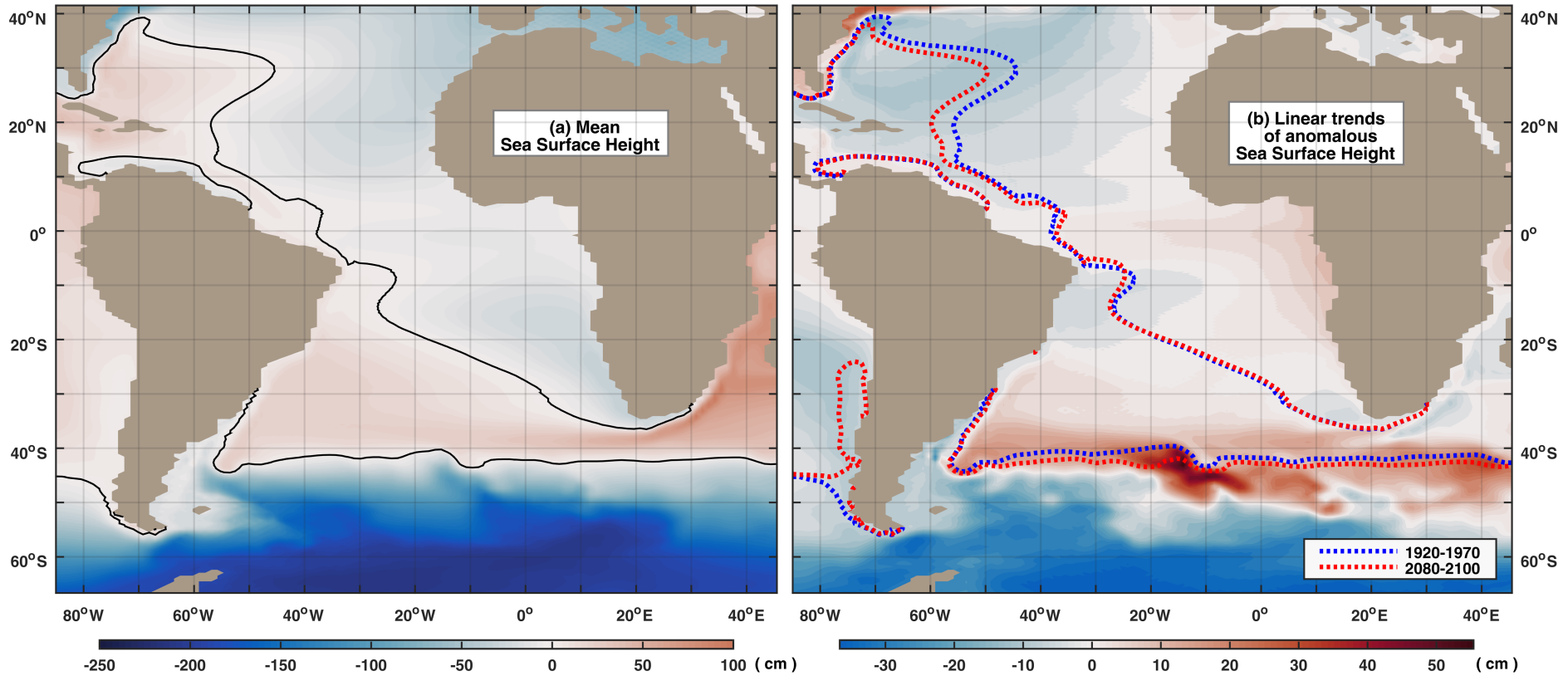


Supplementary Figure 7: | **Sea surface height field - mean and trends (1920-2100)** | **(a)** 1920-2100 mean sea surface height (SSH). Red (blue) represents positive (negative) SSH values and the black filled contour marks the zero SSH line. **(b)** 1920-2100 total trends of SSH anomalies (1920-1970 base period). Red (blue) background colors represent positive/increasing (negative/decreasing) trends, while the red (blue) dotted contour represents the mean 1920-1970 (2080-2100) zero SSH line.

## 7. Supplementary Discussion on *SASG structural changes*:

**(a) SASG northern boundary (sSEC system) at western domains:**
Close to the South American coast (western domain), the three-dimensional SASG structure is dramatically reshaped: in short, its northern boundary (the sSEC) expands meridionally in a depth-dependent way – making its vertical distribution more inclined to the south at upper layers when compared to the mean climatological state. More specifically, the sSEC northernmost limit (represented by the sSEC bifurcation latitude) shifts northward at deeper layers (below ~150 m) – reflecting the increased (decreased) BC (NBUC) transport (article Figure 6); while the sSEC southernmost limit (the zero zonal velocity line separating the sSEC from the SAC) shifts southward entirely (with a bigger shift at the upper layers - article Figure 5) – reflecting a change in the mean direction of the southern sSEC flow, which strengthens and extends further towards the west. The reason for these tilted boundary displacements is that the SBL shift is more closely associated with density-driven flow compensations at deeper layers, linked to AMOC variations (in addition to the fact that wind anomalies seem rather weak near the SBL region); while the shifted direction of the southern sSEC flow is mostly driven by surface wind anomalies that can extend their influence downward through Ekman dynamics (see Figure S6b);

**(b) SASG northern boundary (sSEC system) at central domains:**
Far from the South American coast, between 30°-10°W (central domain), the SASG northern boundary shifts southward entirely (Figure S5a) – both at the north- and southernmost limits –, but the shift at the northern margin occurs along deeper layers, due to the fact that the sSEC system is shrinking to the north, along the outer portions of its bowl-shaped structure (Figure S5d), probably in response to the generalized weakening of the AMOC upper limb – in a larger degree than to wind-forced anomalies;

**(c) Analyzing the shifts of the SASG northernmost edge from west to east:**
At the western domain, the typical bowl-shape of the subtropical gyre tends to flatten – decreasing its southward tilting with depth, since the SBL shifts northward in deeper layers (article Figure 6). Whereas at the central domain of the SASG, the southward tilting of the northern boundary is increased along depth (Figure S5a) – characterizing the generalized shrinking of the sSEC system (Figure S5d), as described above;

**(d) SASG southernmost edge:**
According to the zero SSH and zonally integrated WSC lines, the SASG southern boundary shifts poleward – following hemispheric-scale atmospheric trends (Figures S6c and S7).

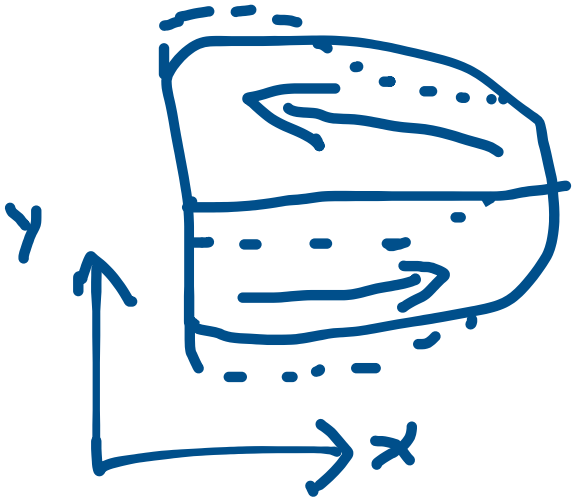


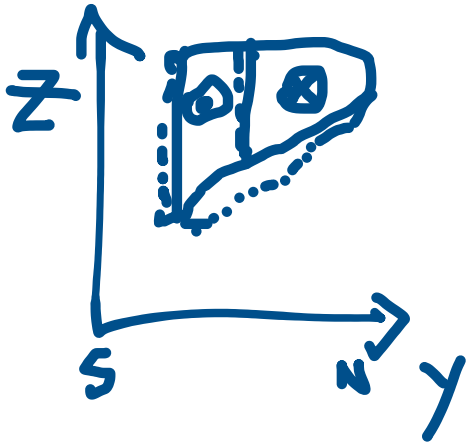

# Weakened AMOC upper limb compensated by strengthened South Atlantic subtropical gyre in CESM1-LE simulations

- Deformed SASG:

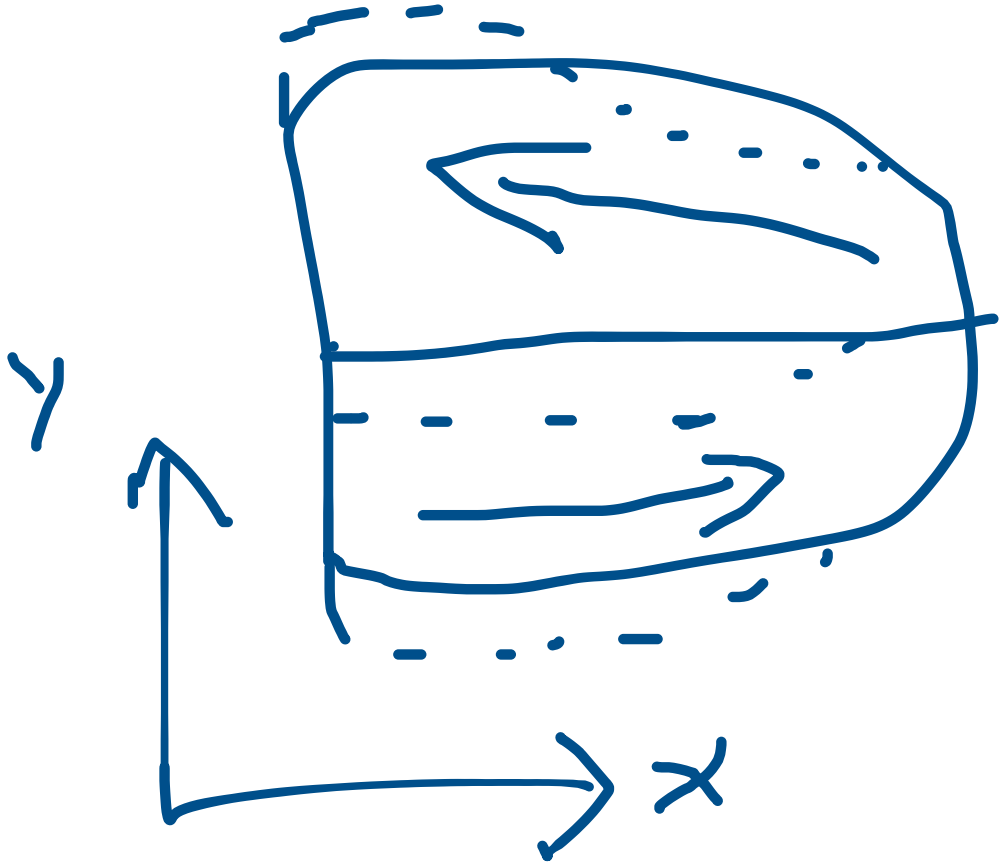


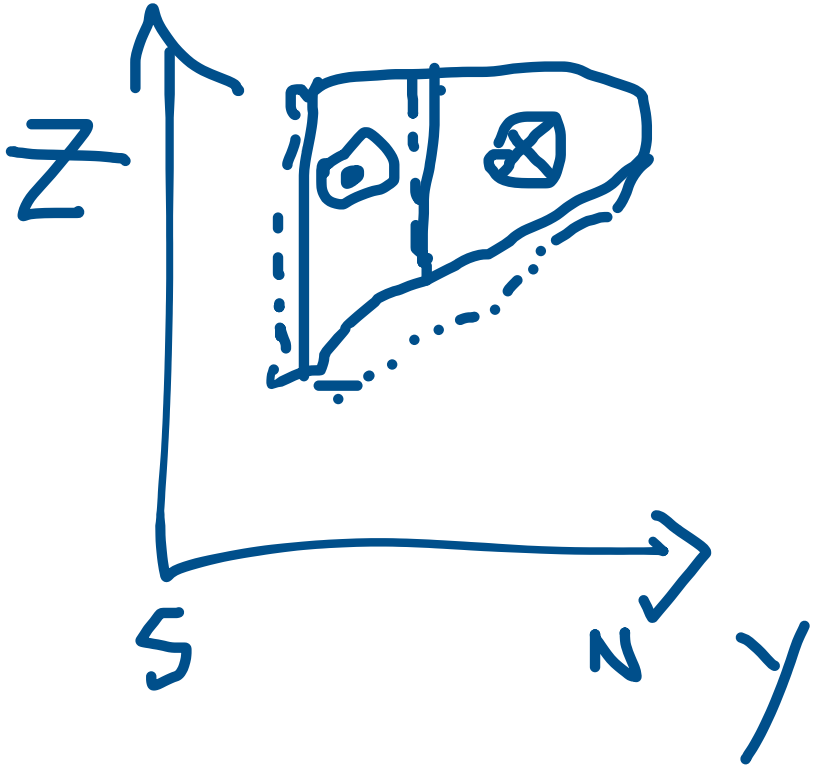

**11. Supplementary Discussion - Agreement between our results and those of previous studies**:

The decreasing southward transport across box (4) in article Figure 2 is consistent with the recent spin-up of the South Pacific subtropical gyre (SPSG)[1–4], linked to an increase of the equatorward transport along its eastern boundary[5]. The reasoning is that less waters escape from the diffuse SPSG southeastern boundary to leak eastward towards the South American coast and join the flow through the DP. Based on mass conservation principles, a spun-up SPSG would increase the anticyclonic gyre transport, advecting more waters to the north at the eastern boundary, and therefore shedding less waters to the east at the southeastern base of the gyre, before closing the anticlockwise circulation loop. Despite the Pacific Ocean being out of our scope, this result also provides indirect evidence for the reported SHSG spin-up[6].

Concerning our simulated change pattern over the AL-BeC-sSEC system (article Figures 1, 2, 4a), it should be noted that our results represent an average of the upper 985-m in the ocean (where SASG and AMOC upper limb pathways predominantly take place — see vertical profiles on Figure S1). Thus, even though the extension of the Agulhas leakage into the South Atlantic is mostly northwestward oriented at the surface layer[7,8], the westward (northward) component of its transport increases (decreases) with depth[7,9], following the subtropical gyre "bowl shape" at the northern boundary.

Accordingly, observational studies have reported a quasi-zonal path extending from the AL region towards the South Atlantic western boundary at intermediate depths[10–13]. The CESM-LE ensemble mean simulates well the mean circulation field and the possibilities of AL-BeC-sSEC pathways across the South Atlantic basin (Figure 1, depicted by the superposing vectors), however, as background colors indicate the trends of the anomalous flow during 1920-2100, this suggests that external forcings are inducing a strengthening of this particular southern zonal route from the AL towards the South Atlantic western boundary into the future.

It is known that the AL amplitude and sensitivity to change might be compromised by inadequate resolution, and that to properly simulate the AL and its nonlinear dynamics an effective resolution of at least 0.1° is needed[14]. Even though, a projected 21st century increase in the AL in response to Southern Hemisphere wind changes was also found with high-resolution ocean models that capture mesoscale processes of the Agulhas system[15–17], in agreement with our results. This suggests that mesoscale processes might be of secondary importance and that changes in basin-scale winds might explain a large component of the projected changes in the AL transport — which may be more reliable than projections for other variables that depend more critically on local processes[18].

Our projected change pattern in the Agulhas system (weakened AC and strengthened AL transport) also resembles one recently found with CMIP5/CMIP6 simulations (see their Figure 1[18]) – where a projected decrease in the AC is shown, whereas the AC westward extension towards the SA intensifies. These authors state that "the westward flowing AC extension south of Africa intensifies in all (28 CMIP5 and 25 CMIP6) models". They also support a projected strengthening of the poleward BC and weakening of the cross-equatorial NBUC-NBC transport.

Also in accordance with our results, it has been shown that a simulated wind-driven increase in the AL happens along with a strengthening of the SASG, which leads to a favored recirculatory route at the SBL, resulting in less AL waters feeding into the NBC as part of the AMOC upper limb[19,20]. In line with that, a projected intensification of the AL linked via interior pathways to an even greater increase in the BC strength (40%) was found with CMIP5 simulations[21], along with a decrease in the northern SA basin interior and the downstream northward NBC transport.

Regarding the ACC-MC system and the Brazil-Malvinas confluence, our results point to an intensification of southern flows associated with the ACC transport from the Pacific across the Atlantic and into the Indian basin (Figures S2-S4), which seems to be associated with atmospheric induced trends, in agreement with some previous studies[22–24]. However, the anthropogenically-forced ACC response is inconsistent across future projections. Because the steeping of isopycnal surfaces induced by strengthened westerlies might either increase the ACC transport through Ekman pumping effects in some models (as described in Section 2.4 of the article) or lead to enhanced (parameterized) eddy-induced transports that act to then reduce the isopycnal slopes in others. The latter process, when acting in combination with a narrowing of the ACC (mainly caused by large poleward shifts of the subtropical gyres), can lead to a reduction in the ACC transport[25] – which in turn might lead to a decreased MC transport and a southward shift of the BMC[26].

Since our simulation results demonstrate a strengthened ACC and MC (article Figures 1, 2), we could not find a consistent southward shift of the Brazil-Malvinas Confluence (BMC)[8,21,26,27] through the horizontal velocity fields, only the zero zonally integrated wind stress curl line depicts a southward shift of the gyre's southern boundary at the BMC region (Figure S6c). Therefore we hypothesize that the strengthened MC might be hampering a southward shift of the BMC influenced by the wind anomalies in the CESM-LE.

In general, our results are in fair agreement with several other simulation and observational results recently reported in the literature. Cyclonic WSC anomalies over the Indian Ocean (Figure Sb) and a projected spin-down of its subtropical gyre coupled to a weakened AC transport are also shown under the RCP8.5 scenario in a warming climate[28]. Based on observational data, a significant southward migration of the SASG southern boundary along 1993-2018 is found[29], though the authors did not find trends in gyre size or strength. In turn, a generalized strengthening of subtropical gyres in all three SH oceans (i.e. the SHSG) has been reported since 1993, using observational data and results from an ocean state estimate[6]. There is observational and model support for a strengthening and poleward movement of global WBCs in attribution to a positive SAM trend[30] – being the only exception the GS, which weakens along with the AMOC. Reanalysis data show that among all three southern subtropical oceans, the impact of SH climate trends over 1978-2002 was larger in the SA, with a 40% increase in the BC transport[1,31].

The CESM-LE shows to reproduce main climate trends according to the literature (e.g. the Southern Hemisphere atmospheric trends) and to predict a weakening of the AMOC as according to a set of CMIP5/CMIP6 model simulations[32].

A wide range of processes of climate variability and change have been explored using the CESM1 Large Ensemble in previous studies[33–37], in good agreement with observations. The Atlantic climate and ocean state in CESM1 and in the Community Climate System Model, version 4 (CCSM4, which contains the same ocean component as CESM1) has also been discussed and compared against observations[38–40].

An extensive evaluation of the CESM1 ocean component (the Parallel Ocean Program version 2, POP2[38]) over the South Atlantic and Southern Ocean[41] shows that the simulated ocean variability over the Southern Hemisphere is dominated by the Southern Annular Mode (consistent with observations) and that the model represents well the frontal zones associated with the Antarctic Circumpolar Current, with their locations being "surprisingly well simulated". However, the ACC transport and the Agulhas leakage are high relative to observations, and the correct location of the Brazil-Malvinas confluence is displaced southward. Since mesoscale features are not explicitly resolved in the model, the representation of some processes that result in water mass formation and interbasin exchanges might be compromised. Most relevant to our work is the fact that the model's relative high viscosity (for compensating its inability to resolve mesoscale processes) produces boundary currents that are too viscous and lack the inertia necessary for retroflection and ring shedding, as in the case of the Agulhas leakage. This overestimates the volume of water exchanged between the Indian and Atlantic Oceans. Still, these authors declare that the amount of Agulhas leakage that reaches the tropical Atlantic is reasonably close to what studies with higher-resolution models have found and that Agulhas leakage variability and trends are reasonably well captured.